Improvement of the photon generation efficiency in phosphorus-doped silicon nanocrystals: Γ–X mixing of the confined electron states

2009 J. Phys.: Condens. Matter 21 045803

(http://iopscience.iop.org/0953-8984/21/4/045803)

J. Phys.: Condens. Matter **21** (2009) 045803 (5pp) doi:10.1088/0953-8984/21/4/045803

Improvement of the photon generation efficiency in phosphorus-doped silicon nanocrystals: Γ–X mixing of the confined electron states

V A Belyakov, A I Belov, A N Mikhaylov, D I Tetelbaum and V A Burdov

University of Nizhniy Novgorod, Nizhniy Novgorod, 603950, Russia

Received 17 November 2008
Published 8 January 2009
Online at stacks.iop.org/JPhysCM/21/045803

Abstract

It has been shown that the central-cell potential of a phosphorus ion embedded in a silicon nanocrystal effectively mixes the electronic states of X- and Γ-bands. Quantum confinement strengthens the Γ–X mixing which, in turn, straightens the nanocrystal's band structure, and substantially intensifies interband radiative recombination.

(Some figures in this article are in colour only in the electronic version)

Incorporation of silicon or silicon-based structures into optoelectronics has remained laborious up to now because of the indirect band gap of silicon. To all appearances, silicon nanocrystals (NCs) are most promising objects for this purpose. The Heisenberg uncertainty relations and phonon assistance make possible interband radiative transitions in Si NCs. Previous calculations [1–4] of phonon-assisted, and no-phonon radiative recombination rates τ_R^{-1} in Si crystallites yielded values varying from 10^5 s^{-1} to 5×10^2 s^{-1} for phonon-assisted, and 1–3 orders of magnitude less for no-phonon transitions, respectively, as the crystallite radius increased from 1 to about 2.5 nm. However, such values are still insufficient for effective photon generation, because competitive nonradiative processes (e.g. capture on dangling bonds, or Auger recombination) are considerably faster. They have rates within the range 10^2–10^{11} s^{-1} depending on the dot size [5] (pp 223, 226). As a result, interband transitions mainly occur through the nonradiative channel. Admittedly, Sykora *et al* [6] reported radiative decay rates τ_R^{-1} equal to 10^7 s^{-1}. However, the NC sizes in their experiments were, presumably, sufficiently small (less than 2 nm in diameter).

As a means of improving emittance of silicon crystallites, doping them with phosphorus is proposed. As reported earlier [7–11], doping with phosphorus can significantly enhance the photoluminescence (PL) intensity from Si NCs. This phenomenon can be explained as being related to the passivation of dangling bonds by phosphorus [7–10], which decreases the nonradiative recombination rate τ_{NR}^{-1}, as well as to factors determining the total amount of light-emitting Si NCs (e.g. impurity-stimulated nucleation/growth of NCs) [11]. Another important factor, which requires special consideration, is the influence of doping directly on the radiative recombination channel. It is the main purpose of our paper to make clear the role of phosphorus in the increase of the radiative recombination rate τ_R^{-1}. We present here our experimental and theoretical results on the PL enhancement due to P-doping in silicon NCs embedded in a SiO_2 matrix.

In order to study experimentally the effect of phosphorus on the light-emitting properties of Si quantum dots, both spectral and temporal characteristics of PL in the range of 600–900 nm were measured for SiO_2 layers with Si NCs embedded. The ensemble of NCs with a mean diameter of 3.5 nm was synthesized in thermally grown SiO_2 films (800 nm thick) by Si^+ ion implantation (ion dose—7×10^{16} cm^{-2}, ion energy—100 keV) with subsequent annealing for 2 h at 1000 °C in a N_2 atmosphere. Before annealing, some of the samples were implanted with P^+ ions (100 keV) with doses in the range of 10^{14}–10^{17} cm^{-2} (corresponding to the range of phosphorus peak concentrations of 10^{19}–10^{22} cm^{-3}). Measurement of the PL spectra was carried out at room temperature by using the 337 nm line of a pulsed N_2 laser (mean power of ∼ 10 mW, pulse duration t_p ∼ 10 ns, pulse repetition rate—25 Hz) for PL excitation, a grating monochromator (Acton SP-150) and a photomultiplier tube (Hamamatsu R-928) for PL detection. The excitation power was chosen to lie in the linear region of the PL signal power dependency. PL decay curves were

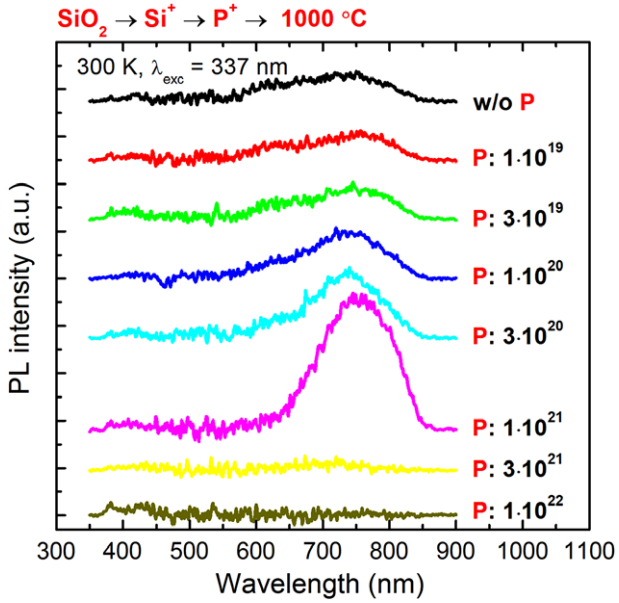

Figure 1. PL spectra of Si^+-implanted SiO_2 films synthesized at 1000 °C after irradiation with P^+ and final annealing at 1000 °C. Numeral markers indicate the ion concentrations in cm^{-2}.

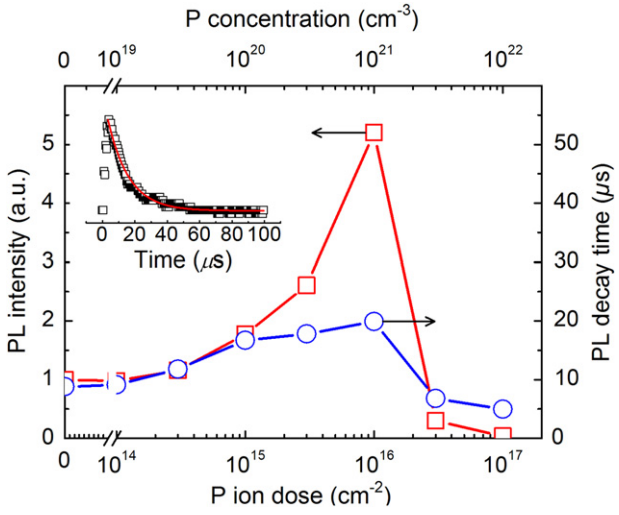

Figure 2. Phosphorus concentration (dose) dependencies of PL intensity and decay time measured at 750 nm. The inset shows temporal behaviour of the PL signal at P-dose of 10^{16} cm^{-2}.

measured at the wavelength of 750 nm (the maximum of the PL spectrum) by using an SRS Boxcar Averager & Fast Gate Integrator.

The NC-related PL spectra are shown in figure 1. The PL intensity monotonically rises with increasing P-dose up to 10^{16} cm^{-2} and drops at the higher doses. The PL quenching can be a consequence of some destructive mechanisms of phosphorus precipitation, and Auger recombination. At phosphorus doses close to 10^{16} cm^{-2}, the PL intensity peak rises up to 5–6 times compared to the case of undoped NCs, as seen in figure 2, where the PL intensities and lifetimes $\tau_{PL} = \tau_{NR}\tau_R/(\tau_{NR} + \tau_R)$ measured at 750 nm are plotted as functions of the phosphorus ion dose (concentration). It is worth noting that the PL lifetime τ_{PL} changes slowly in the dose range (from 10^{15} to 10^{16} cm^{-2}) where the PL intensity grows rapidly with phosphorus concentration. A possible explanation is that the PL decay (typical time-dependence is presented in the inset to figure 2) is determined by the balance of radiative and nonradiative processes as a result of passivation of the interface dangling bonds, whereas the intensity of the PL is proportional to the rate τ_R^{-1} at the almost constant value of τ_{PL}.

Below, we shall theoretically show that doping can substantially improve the radiative channel efficiency in Si NCs. In particular, doping increases the radiative decay rate τ_R^{-1}, which, in turn, increases the quantum yield and the PL intensity. In what follows, within the framework of envelope function approximation, we calculate the lifetime of radiative interband transition in the NC with a phosphorus ion, and analyse the lifetime dependence on the ion position in the NC.

Earlier, Iory *et al* [12] calculated the imaginary part $\varepsilon''(\omega)$ of the dielectric function for a P-doped 1.5 nm silicon NC by first-principles methods. In contrast to this work [12], we are interested in optical transitions in NCs whose sizes are greater than 2 nm. Moreover, the use of the imaginary part $\varepsilon''(\omega)$ is more convenient for calculations of absorption spectra than of emission spectra. We suppose that main contribution to the emission spectrum of the NC comes from the basic interband electron transitions between the ground conduction and valence states. For this reason, we shall compute the radiative lifetimes for these transitions only.

Coulomb interaction of the excited electron with the phosphorus ion plays a crucial role in the recombination process. The Coulomb field consists of two parts: the long-range hydrogen-like term V; and the short-range microscopic term W (the so-called central-cell field [13]).

The hydrogen-like part which, for bulk silicon, is written as $V(r) = -e^2/\varepsilon_s r$, with ε_s being the silicon permittivity, is transformed in the NC into the sum $V(\mathbf{r}) = V_{sp}(r) + V_{ie}(\mathbf{r})$ due to the appearance of polarization charges at the NC boundary. Here

$$V_{sp}(r) = \frac{e^2(\varepsilon_s - \varepsilon_d)}{2\varepsilon_s R}\sum_{l=0}^{\infty}\frac{l+1}{l\varepsilon_s + (l+1)\varepsilon_d}\frac{r^{2l}}{R^{2l}} \qquad (1)$$

is the self-polarization potential energy originating from the interaction between the electron and its own image. ε_d is the permittivity of the wide-band dielectric matrix surrounding the NC, and R stands for the NC radius. The term $V_{ie}(\mathbf{r}, \mathbf{h})$ describes the direct electron–ion interaction, as well as the interaction of the electron with the ion image:

$$V_{ie}(\mathbf{r}, \mathbf{h}) = -\frac{e^2}{\varepsilon_s|\mathbf{r} - \mathbf{h}|} - \frac{e^2(\varepsilon_s - \varepsilon_d)}{\varepsilon_s R} \times \sum_{l=0}^{\infty}\frac{h^l r^l}{R^{2l}}\frac{l+1}{l\varepsilon_s + (l+1)\varepsilon_d}P_l(\cos\theta), \qquad (2)$$

where $\mathbf{h}$ is the donor position vector, $P_l(\cos\theta)$ is the Legendre polynomial, and θ is the angle between $\mathbf{r}$ and $\mathbf{h}$.

The short-range part W can be determined using the microscopic dielectric function obtained by Walter and Cohen [14] with the empirical pseudo-potential method, as

follows:

$$W(\mathbf{r},\mathbf{h}) = -\frac{e^2}{|\mathbf{r}-\mathbf{h}|}\left[A\exp\left(-\alpha|\mathbf{r}-\mathbf{h}|\right) + \left(1 - A - \frac{1}{\varepsilon_s}\right) \times \exp(-\beta|\mathbf{r}-\mathbf{h}|)\right]. \quad (3)$$

Here, α and β equal 0.82 and 5.0 of the reciprocal Bohr radius, respectively, and $A = 1.142$. Pantelides and Sah [15] have obtained a similar expression earlier. They also found that the existence of the local short-range field is an inherent property of an isocoric impurity, such as phosphorus. All other impurities produce nonlocal and stronger perturbations, the description of which within the kp-method is questionable. The PL enhancement discussed in the present paper is exclusively due to the short-range field of phosphorus, as will be shown below.

Determination of the electronic structure of a P-doped silicon crystallite also exhibits a key role of the short-range field in the electron state formation [16–20]. In particular, in the conduction band, the spinless ground state (being sixfold degenerate in an undoped dot) splits due to the short-range field, in a way similar to that of bulk Si, into a singlet with the lowest energy, and doublet and triplet groups of states. Such a splitting occurs independently of the donor position in the dot. The wavefunctions ψ_I of the two (if spin is taken into account) ground states, being initial (I) ones under the basic radiative transition, have the form [19]:

$$|\psi_I\rangle \equiv |\psi_\sigma\rangle = |\sigma\rangle \sum_{X_1,b} \lambda_b(X_1)|X_1\rangle|b\rangle. \quad (4)$$

Here, $|\sigma\rangle = |\uparrow\rangle, |\downarrow\rangle$, $\lambda_b(X_1)$ are the expansion coefficients, $|X_1\rangle$ are the Bloch functions of the representation X_1 of the X-point built in accordance with the symmetry of the irreducible representations A_1, E, and T_2 of the tetrahedral group T_d. The Bloch function $|A_1\rangle \equiv u_A(\mathbf{r})$ describes the singlet state in the bulk silicon, while $|E^{(1,2)}\rangle \equiv u_E^{(1,2)}(\mathbf{r})$, and $|T_2^{(1,2,3)}\rangle \equiv u_T^{(1,2,3)}(\mathbf{r})$ are the doublet, and triplet functions, respectively. Function $|A_1\rangle$ has a nonzero value at the donor site in contrast to the functions $|E^{(1,2)}\rangle$, and $|T_2^{(1,2,3)}\rangle$, which equal zero [13]. Index b stands for the s-, and p-type envelope functions of the isotropic zero-order k–p Hamiltonian (see [19] for details). These functions are written as

$$|s\rangle \equiv \phi(r) = \sqrt{\frac{\pi}{2R^3}}\, j_0(\pi r/R),$$
$$|p_a\rangle \equiv \phi_a(\mathbf{r}) = \sqrt{\frac{3}{2\pi R^3}}\,\frac{j_1(\mu r/R)}{j_0(\mu)}\,\frac{x_a}{r}, \quad (5)$$

where $a = 1, 2, 3$ (or x, y, z), $j_{0,1}(x)$ are spherical Bessel functions, and μ is the first root of $j_1(x)$.

In the case of a central located donor inside the NC, coefficient $\lambda_s(A_1)$ is close to 1, while all the other coefficients are negligibly small [19]. As a result, wavefunctions of the two initial states, differing by spin projection, can be represented approximately by: $|\psi_\sigma\rangle \approx |A_1\rangle|s\rangle|\sigma\rangle$. If the donor position is asymmetric, all the coefficients $\lambda_b(X_1)$ should be taken into account in the expansion (4). In this case, the portions of all Bloch and envelope functions are determined numerically [19].

In the valence band no splitting, other than the spin–orbit one, arises until the donor occupies the dot centre. In this case, the short-range field results only in a shift of the energy levels. The upper energy level in the valence band is fourfold degenerate. Wavefunctions ψ_F of this quadruplet (final (F) electron states or, equally, initial hole states) are the products of the Luttinger functions $|M\rangle$ of the total angular momentum 3/2 with $M = \pm 1/2, \pm 3/2$, and the s-type envelope function: $|\psi_F\rangle \equiv |\psi_M\rangle = |M\rangle|s\rangle$ [21]. If the donor position is asymmetric, M is no longer a good quantum number. In this case, the upper quadruplet splits into two doublets whose wavefunctions have rather cumbrous expressions [22]. We do not cite them here. Nevertheless, it is possible to write them in some general form similar to that for the initial state (equation (4)):

$$|\psi_F\rangle = \sum_{\Gamma_{25'},b,\sigma} \lambda_{b\sigma}(\Gamma_{25'})|\Gamma_{25'}\rangle|b\rangle|\sigma\rangle. \quad (6)$$

Here, $|\Gamma_{25'}\rangle$ denotes one of three basic Bloch functions $|YZ\rangle$, $|XZ\rangle$, or $|XY\rangle$ of the spinless irreducible representation $\Gamma_{25'}$ of the Γ-point. All these Bloch functions equal zero at the donor site. Coefficients $\lambda_{b\sigma}(\Gamma_{25'})$ have been found earlier [21].

Let us compute the transition rates $\tau_R^{-1}(I, F)$ between all possible I and F states. In order to compute the rates we employ the Fermi golden rule. After some algebra, it can be written in the following form:

$$\tau_R^{-1}(I, F) = \frac{4e^2\kappa(\varepsilon_s;\varepsilon_d)\varepsilon_g(R)}{3m_0^2\hbar^2c^3}|\mathbf{p_{IF}}|^2. \quad (7)$$

Here, e and m_0 are the free-electron charge and mass, respectively, $\varepsilon_g(R)$ is the NC's gap depending on the dot radius, $\hbar$ is the Plank constant, c stands for the speed of light in a vacuum, and $\mathbf{p_{IF}}$ is the optical momentum matrix element. The function $\kappa(\varepsilon_s;\varepsilon_d) = 9\varepsilon_d^{5/2}/(2\varepsilon_d + \varepsilon_s)^2$ replaces the standard factor $\sqrt{\varepsilon_s}$ due to the replacement of the homogeneous media with bulk permittivity ε_s by a spherical silicon nanocrystal surrounded by a dielectric wide-band matrix with a dielectric constant ε_d [22].

In the case of indirect transition, $\mathbf{p_{IF}}$ is usually close to zero. As a result, the no-phonon radiative decay rate turns out to be small. However, the presence of the phosphorus ion, creating the short-range field in the NC, drastically changes the situation. The central-cell potential, being of the short-range type in a real space, turns into the long-range one in a momentum space. Correspondingly, it can mix the Bloch states of distant points in the Brillouin zone, such as, e.g., nonequivalent X-points in the conduction band of silicon [13] (X–X mixing called usually as a valley–orbit interaction), or X- and Γ-points (Γ–X mixing). The latter crucially influences the optical matrix element and the decay rate. The Γ–X mixing involves Bloch states $|\Gamma_{15}\rangle$ and $|\Gamma_{2'}\rangle$ in the initial electron states $|\psi_I\rangle$, and the Bloch states $|X_4\rangle$ in $|\psi_F\rangle$, as shown schematically in figure 3. The presence of the Bloch states $|\Gamma_{15}\rangle$ and $|\Gamma_{2'}\rangle$, and $|X_4\rangle$ in the modified initial electron, and hole states, respectively, transforms the electron–hole indirect transition into partly direct. This significantly accelerates the interband radiative transitions.

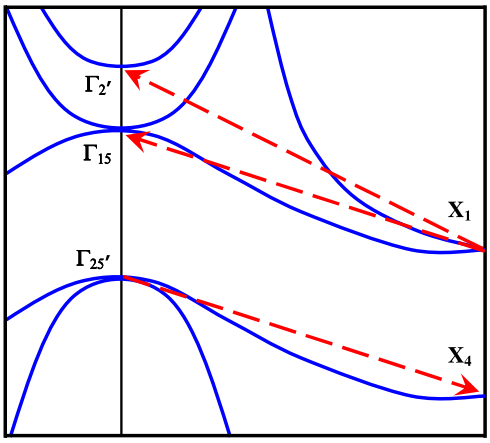

Figure 3. Schematic representation of the silicon band structure. Dashed arrows indicate mixing the initial/final electron state (band $X_1/\Gamma_{25'}$) with the intermediate states from the bands Γ_{15}, $\Gamma_{2'}/X_4$.

Thus, the short-range donor field mixes the initial $|\psi_I\rangle$, or the final $|\psi_F\rangle$, electron states with the so-called intermediate states $|\psi_i^{(I)}\rangle$, or $|\psi_i^{(F)}\rangle$, having Bloch functions $|\Gamma_{15}\rangle$ and $|\Gamma_{2'}\rangle$, or $|X_4\rangle$, respectively. We neglect all the other X- and Γ-bands with too low or too high energies. Taking into account the short-range Coulomb field as a first-order perturbation, one can modify the wavefunctions of the initial and final electron states as follows:

$$|\Psi_{I,F}\rangle = |\psi_{I,F}\rangle + \sum_i C_{I,F}(i)|\psi_i^{(I,F)}\rangle. \tag{8}$$

Here, $C_{I,F}(i) = \langle\psi_i^{(I,F)}|W|\psi_{I,F}\rangle/(\varepsilon_{I,F} - \varepsilon_i)$ are the amplitude coefficients of the intermediate states arising due to the donor field, with $\varepsilon_{I,F}$ and ε_i being the energies of the initial/final and intermediate states, respectively. For convenience, one can represent wavefunctions of the intermediate states $|\psi_i^{(I,F)}\rangle$ in a form similar to $|\psi_I\rangle$ or $|\psi_F\rangle$:

$$|\psi_i^{(I,F)}\rangle = \sum_{\Lambda,b,\sigma} \lambda_{b\sigma}(\Lambda)|\Lambda\rangle|b\rangle|\sigma\rangle, \tag{9}$$

where $|\Lambda\rangle$ are the Bloch functions of representations Γ_{15} and $\Gamma_{2'}$ for $|\psi_i^{(I)}\rangle$, and X_4 for $|\psi_i^{(F)}\rangle$. Expansion coefficients $\lambda_{b\sigma}(\Lambda)$ are determined as solutions of eigenvector and eigenvalue problem for the k–p Hamiltonian operators in Γ_{15}, $\Gamma_{2'}$, and X_4 bands.

It is important to emphasize that the Bloch functions $|\Gamma_{15}\rangle$ and $|X_4\rangle$ equal zero at the donor site while $|\Gamma_{2'}\rangle$ has some finite value (see, e.g., subsection IID2 of the book by Yu and Cardona [23]). Since the short-range Coulomb interaction differs from zero in the vicinity nearest to the donor nucleus, the coefficients $C_I(\Gamma_{15})$ and $C_F(X_4)$ have to be much less than $C_I(\Gamma_{2'})$. Therefore, we neglect $C_I(\Gamma_{15})$ and $C_F(X_4)$ in the subsequent calculations. However, $C_I(\Gamma_{2'})$ should be kept in equation (8). As a result, the wavefunction of the final electron state remains invariable: $|\Psi_F\rangle = |\psi_F\rangle$; while the wavefunction of the initial state is modified by the short-range donor field: $|\Psi_I\rangle = |\psi_I\rangle + C_I(\Gamma_{2'})|\psi_{\Gamma_{2'}}\rangle$, where $|\psi_{\Gamma_{2'}}\rangle$ is the wavefunction in the band $\Gamma_{2'}$.

Since $\Gamma_{2'}$ is a simple band, it is possible to describe the electron states in this band with a standard effective mass approximation as a product of the corresponding Bloch function $\Gamma_{2'}$ and some envelope function. In particular, if the donor distribution in the NC has spherical symmetry, the ground state in the $\Gamma_{2'}$-band has an envelope function of s-type and the total wavefunction $|\psi_{\Gamma_{2'}}\rangle = |\Gamma_{2'}\rangle|s\rangle$. All other states in the $\Gamma_{2'}$-band have p-, d-, 2s-type, etc envelope functions, and contribute slightly to the Γ–X mixing. In the case of an asymmetric donor distribution, the envelope function of the ground state in the $\Gamma_{2'}$-band will be predominantly a result of s-p hybridization. Then the expression for the wavefunction of the intermediate state (equation (9)) is transformed into $|\psi_{\Gamma_{2'}}\rangle = |\Gamma_{2'}\rangle|\sigma\rangle\sum_b \lambda_b(\Gamma_{2'})|b\rangle$, where the index b runs over s, p_x, p_y, and p_z.

Consequently, we have to determine the only coefficient $C_I(\Gamma_{2'}) = \langle\psi_{\Gamma_{2'}}|W|\psi_I\rangle/(\varepsilon(A_1) - \varepsilon(\Gamma_{2'}))$ for the ground state in the $\Gamma_{2'}$-band. Here, $\varepsilon(A_1)$ is the energy of the initial state—the ground state in the X_1-band. To calculate the matrix element $\langle\psi_{\Gamma_{2'}}|W|\psi_I\rangle$ we employ equation (3) for W, and the free-electron model with Bloch functions represented by the plane waves [23]. Energies $\varepsilon(A_1)$ and $\varepsilon(\Gamma_{2'})$, as well as expansion coefficients $\lambda_b(\Gamma_{2'})$, can be found analytically in the case of the central located donor (see, e.g., [19] for the initial state). Otherwise, the energies and expansion coefficients are determined numerically.

It should be noted that the total decay rate $\tau_R^{-1}(I,F)$ consists of two parts. The first part is the rate $\tau_D^{-1}(I,F)$ of the donor-induced transitions, while the second part represents the rate $\tau_{ph}^{-1}(I,F)$ of the phonon-assisted transitions. The latter was previously computed and found to be decreasing with doping [4]. The donor-induced contribution was not calculated earlier. We have calculated $\tau_D^{-1}(I,F)$ as well as the rate τ_D^{-1} being average over all possible I → F transitions for the different degenerate initial and final states.

According to the Fermi golden rule, the rate of the no-phonon radiative transitions induced by the short-range donor field is defined by the squared magnitude of $|\mathbf{p_{IF}}| \equiv p_{IF} = p_{cv}|C_I(\Gamma_{2'})|$. Here, p_{cv} is the so-called momentum matrix element usually arising in the Fermi golden rule for direct electron transitions. In the frames of the free-electron model, p_{cv} equals $2\pi\hbar/a_0$, where a_0 stands for the silicon lattice constant. For indirect transitions in silicon crystallites, the optical matrix element p_{IF} acquires an additional small factor $C_I(\Gamma_{2'})$ close to 0.1 for 2–3 nm crystallites, and decreasing as the NC size increases.

Figure 4 presents the dependence of the decay rates on the dot radius for the case where the phosphorus ion occupies the dot centre ($h = 0$). The initial and final states, and the rates, can be symbolically denoted by σ and M, and $\tau_R^{-1}(\sigma, M)$, respectively. In this case it is possible to show that six of the eight $\sigma \to M$ electron transitions are allowed, and their rates obey the following equalities: $\tau_D^{-1}(\uparrow, 3/2) = \tau_D^{-1}(\downarrow, -3/2) \equiv 2\tau_D^{-1}$; $\tau_D^{-1}(\uparrow, 1/2) = \tau_D^{-1}(\downarrow, -1/2) \equiv 4\tau_D^{-1}/3$; $\tau_D^{-1}(\uparrow, -1/2) = \tau_D^{-1}(\downarrow, 1/2) \equiv 2\tau_D^{-1}/3$. Two residual transitions $|\uparrow\rangle \to |-3/2\rangle$ and $|\downarrow\rangle \to |3/2\rangle$ are spin-forbidden. The rates of all the six allowed transitions, as well as the average rate, are depicted in the figure. One can see

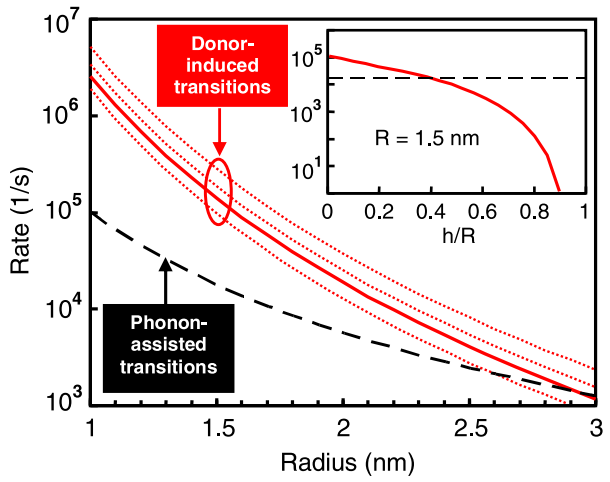

Figure 4. Rates of the donor-induced allowed radiative transitions versus the dot size at $h = 0$ (from bottom to top): $\tau_D^{-1}(\uparrow, -1/2) = \tau_D^{-1}(\downarrow, 1/2)$; $\tau_D^{-1}(\uparrow, 1/2) = \tau_D^{-1}(\downarrow, -1/2)$; $\tau_D^{-1}(\uparrow, 3/2) = \tau_D^{-1}(\downarrow, -3/2)$—dots; their average rate τ_D^{-1}—solid line. Average rate τ_0^{-1} of the phonon-assisted transition in undoped crystallite (according to [4])—dashed line. Inset: decay rate τ_D^{-1} as a function of dimensionless donor displacement from the dot centre h/R—solid line. The horizontal dashed line represents τ_0^{-1}.

that in a wide range of dot sizes, the donor-induced radiative transitions turn out to be faster than the phonon-assisted ones, whose average rate τ_0^{-1}, for the case of undoped NC [4], is shown with a dashed line. This trend is more pronounced for smaller sizes; e.g., at $R = 1$ nm, τ_D^{-1} exceeds the average rate τ_0^{-1} by more than an order of magnitude.

This is a direct consequence of the quantum confinement, which becomes stronger for smaller NCs. The matrix element $\langle\psi_{\Gamma_{2'}}|W|\psi_\sigma\rangle$, defining the amplitude of the direct transition $\Gamma_{2'} \to \Gamma_{25'}$, is proportional to the squared value of the s-type envelope function (equation (5)) at $\mathbf{r} = \mathbf{h}$. The latter is due to the short-range character of W. Because we discuss the central located donor, then $\mathbf{h} = 0$, and $\langle\psi_{\Gamma_{2'}}|W|\psi_\sigma\rangle \sim R^{-3}$ according to equation (5) and explicit expressions for $|\psi_{\Gamma_{2'}}\rangle$ and $|\psi_\sigma\rangle$. Correspondingly, $\tau_D^{-1}(\sigma, M)$ is proportional to R^{-6}, and rises sharply as the NC size decreases. At the same time, τ_0^{-1} rises as R^{-3} [4] with decreasing R, and turns out to be less than τ_D^{-1} at small sizes.

As has already been mentioned above, the no-phonon indirect transitions in undoped NC are 1–3 orders of magnitude slower than the phonon-assisted ones. This is why we compare here τ_D^{-1} with the phonon-assisted decay rate but not with the rate of the no-phonon indirect transitions.

We should note, however, that such a relationship between τ_D^{-1} and τ_0^{-1} turns into the opposite one if the donor shifts towards the NC surface, see inset of figure 4. Beyond half the dot radius, the average decay rate τ_D^{-1} drops with increasing h. The origin of this sharp decrease lies in a strong weakening the central-cell interaction near the dot boundary, and the wavefunction reconstruction leading to a certain spatial separation of the electron densities in the conduction and valence bands. In particular, electron density in the conduction band tends to accumulate near the donor, while the valence band density tends to occupy donor-free areas. Thus, the donor-induced radiative recombination substantially decelerates as the system asymmetry rises.

Nevertheless, it is seen that some finite-size area exists around the NC's centre, where doping is efficient from the point of view of considerable acceleration of the radiative interband recombination in Si NCs, leading to the enhancement of the PL intensity. We would like to emphasize once more that such an enhancement is possible due to improvement of the radiative channel efficiency, which is mainly caused by the short-range Coulomb field of the phosphorus ion.

Acknowledgments

We are grateful to I N Yassievich for helpful discussions. The authors thank as well the 'Dynasty' Foundation (Russia), and the Russian Ministry of Education for financial support through the program RNP. One of the authors (ANM) acknowledges support in the form of a CRDF Fellowship (Y4-P-01-05).

References

[1] Hybertsen M S 1994 *Phys. Rev. Lett.* **72** 1514
[2] Delerue C, Allan G and Lannoo M 2001 *Phys. Rev.* B **64** 193402
[3] Moskalenko A S, Berakdar J, Prokofiev A A and Yassievich I N 2007 *Phys. Rev.* B **76** 085427
[4] Belyakov V A, Burdov V A, Lockwood R and Meldrum A 2008 *Adv. Opt. Technol.* **2008** 279502
[5] Delerue C and Lannoo M 2004 *Nanostructures: Theory and Modelling* (Berlin: Springer)
[6] Sykora M, Mangolini L, Schaller R D, Kortshagen U, Jurbergs D and Klimov V I 2008 *Phys. Rev. Lett.* **100** 067401
[7] Tetelbaum D I, Karpovich I A, Stepikhova M V, Shengurov V G, Markov K A and Gorshkov O N 1998 *Surf. Investig. X-ray, Sinchrotron Neutron Tech.* **14** 601
[8] Fujii M, Mimura A, Hayashi S and Yamamoto K 1999 *Appl. Phys. Lett.* **75** 184
[9] Mimura A, Fujii M, Hayashi S, Kovalev D and Koch F 2000 *Phys. Rev.* B **62** 12625
[10] Tetelbaum D I, Trushin S A, Burdov V A, Golovanov A I, Revin D G and Gaponova D M 2001 *Nucl. Instrum. Methods* B **174** 123
[11] Mikhaylov A N, Tetelbaum D I, Burdov V A, Gorshkov O N, Belov A I, Kambarov D A, Belyakov V A, Vasiliev V K, Kovalev A I and Gaponova D M 2008 *J. Nanosci. Nanotechnol.* **8** 780
[12] Iori F, Degoli E, Luppi E, Magri R, Marri I, Cantele G, Ninno D, Trani F and Ossicini S 2006 *J. Lumin.* **121** 335
[13] Kohn W and Luttinger J M 1955 *Phys. Rev.* **97** 1721
[14] Walter J P and Cohen M L 1970 *Phys. Rev.* B **2** 1821
[15] Pantelides S T and Sah C T 1974 *Phys. Rev.* B **10** 621
[16] Melnikov D V and Chelikowsky J R 2004 *Phys. Rev. Lett.* **92** 046802
[17] Zhou Z, Steigerwald M L, Friesner R A, Brus L and Hybertsen M S 2005 *Phys. Rev.* B **71** 245308
[18] Xu Q, Luo J W, Li S S, Xia J B, Li J and Wei S H 2007 *Phys. Rev.* B **75** 235304
[19] Belyakov V A and Burdov V A 2007 *Phys. Rev.* B **76** 045335
[20] Ramos L E, Degoli E, Cantele G, Ossicini S, Ninno D, Furthmuller J and Bechstedt F 2007 *J. Phys.: Condens. Matter* **19** 466211
[21] Belyakov V A and Burdov V A 2008 *J. Phys.: Condens. Matter* **20** 025213
[22] Thranhardt A, Ell C, Khitrova G and Gibbs H M 2002 *Phys. Rev.* B **65** 035327
[23] Yu P Y and Cardona M 2002 *Fundamentals of Semiconductors. Physics and Materials Properties* (Berlin: Springer)